Optogenetic downregulation of protein levels with an ultrasensitive switch

Sophia Hasenjäger*, Jonathan Trauth*, Sebastian Hepp, Juri Goenrich, Lars-Oliver Essen and Christof Taxis

*these authors contributed equally

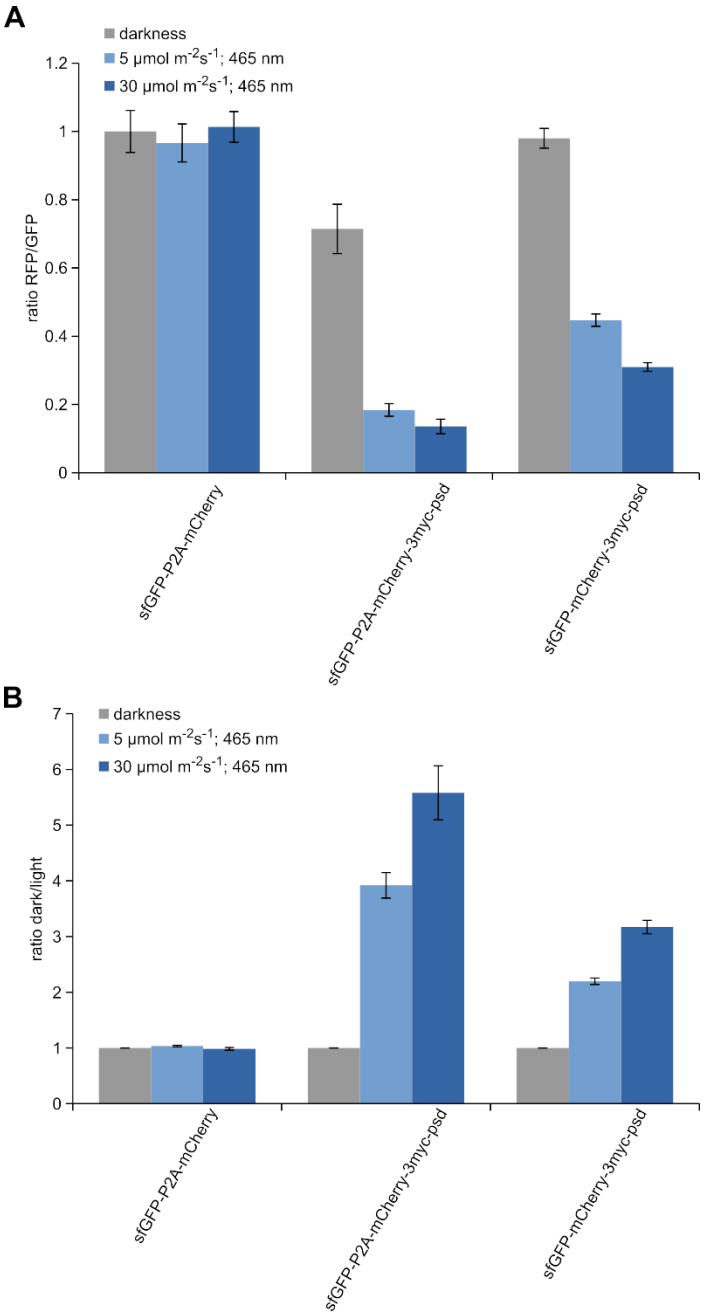

Supplemental Figure S1 Ratiometric measurement of psd abundance.

A) Quantification of RFP fluorescence in relation to GFP abundance in yeast cells (ESM356-1) carrying plasmids pFMI14 (sfGFP-P2A-mCherry), pDS185 (sfGFP-P2A-mCherry-3myc-psd), and pDS194 (sfGFP-mCherry-3myc-psd) was done by fluorimeter measurements (n=6; error bars SEM). B) Dark/light ratios of the data shown in **A**. The separation of sfGFP and mCherry-psd by the viral P2A sequence (sfGFP-mCherry-3myc-psd) results in a higher dark/light ratio as direct fusion of the fluorophores (sfGFP-mCherry-3myc-psd). Stable fluorescence proteins are not influenced by blue-light (sfGFP-P2A-mCherry).

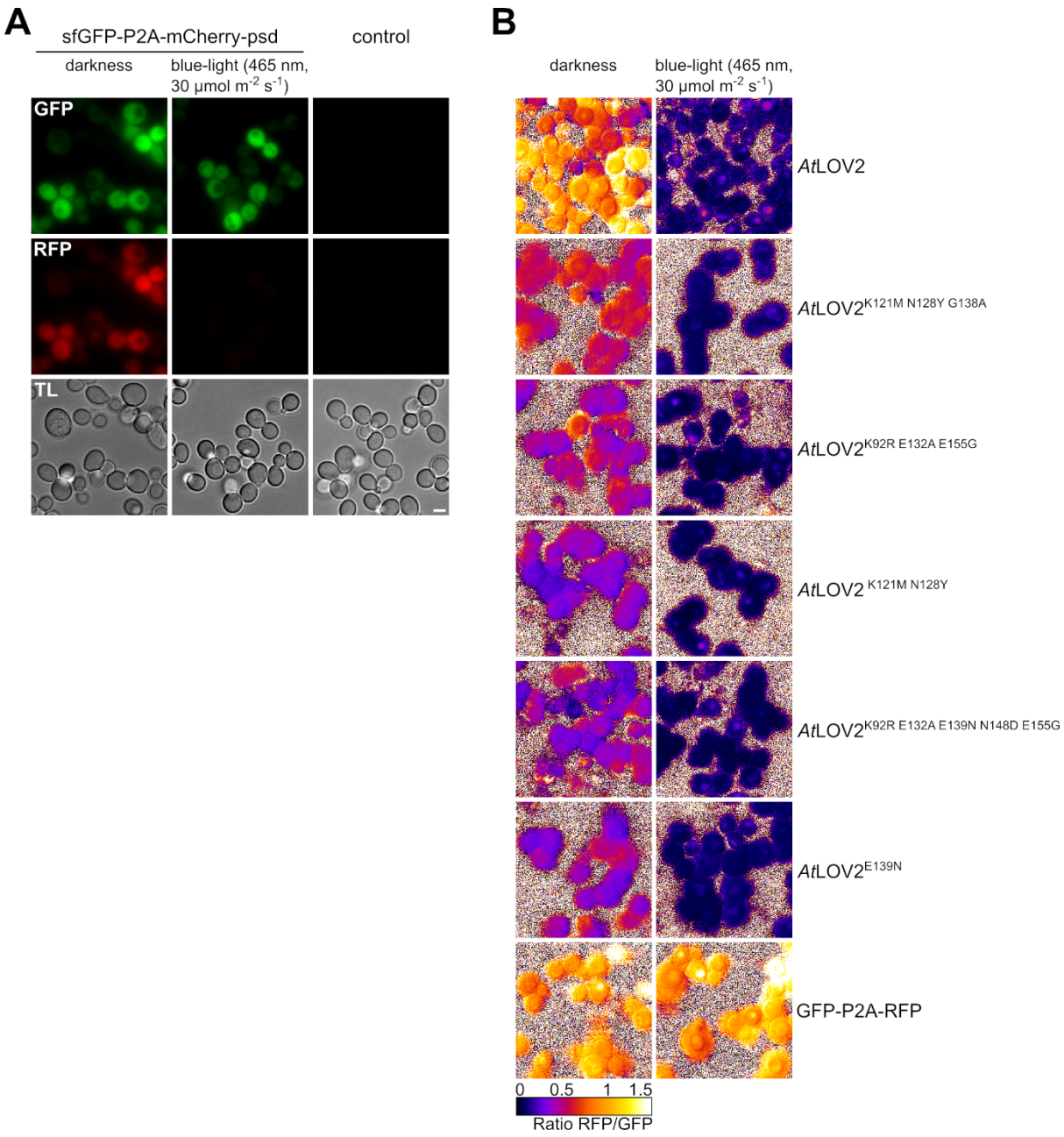

Supplemental Figure S2 Ratiometric measurement of psd abundance by fluorescence microscopy.

A) Fluorescence microscopy images of sfGFP-P2A-mCherry-psd (pDS185) in ESM356-1 cells in darkness and in cells exposed to blue-light. Control cells ESM356-1 containing pRS315 (bar size 2 µm). B) RFP/GFP ratiometric images of different psd constructs (as indicated) in the context of the sfGFP-mCherry-3myc-psd constructs. False colors indicate high ratio (white to yellow, high mCherry abundance) or low ratio (blue to black color; low mCherry abundance) Plasmids used in ESM356-1 (top to bottom): pDS185; pSH11; pSH5; pSH7; pSH1; pSH8; pFMI14.

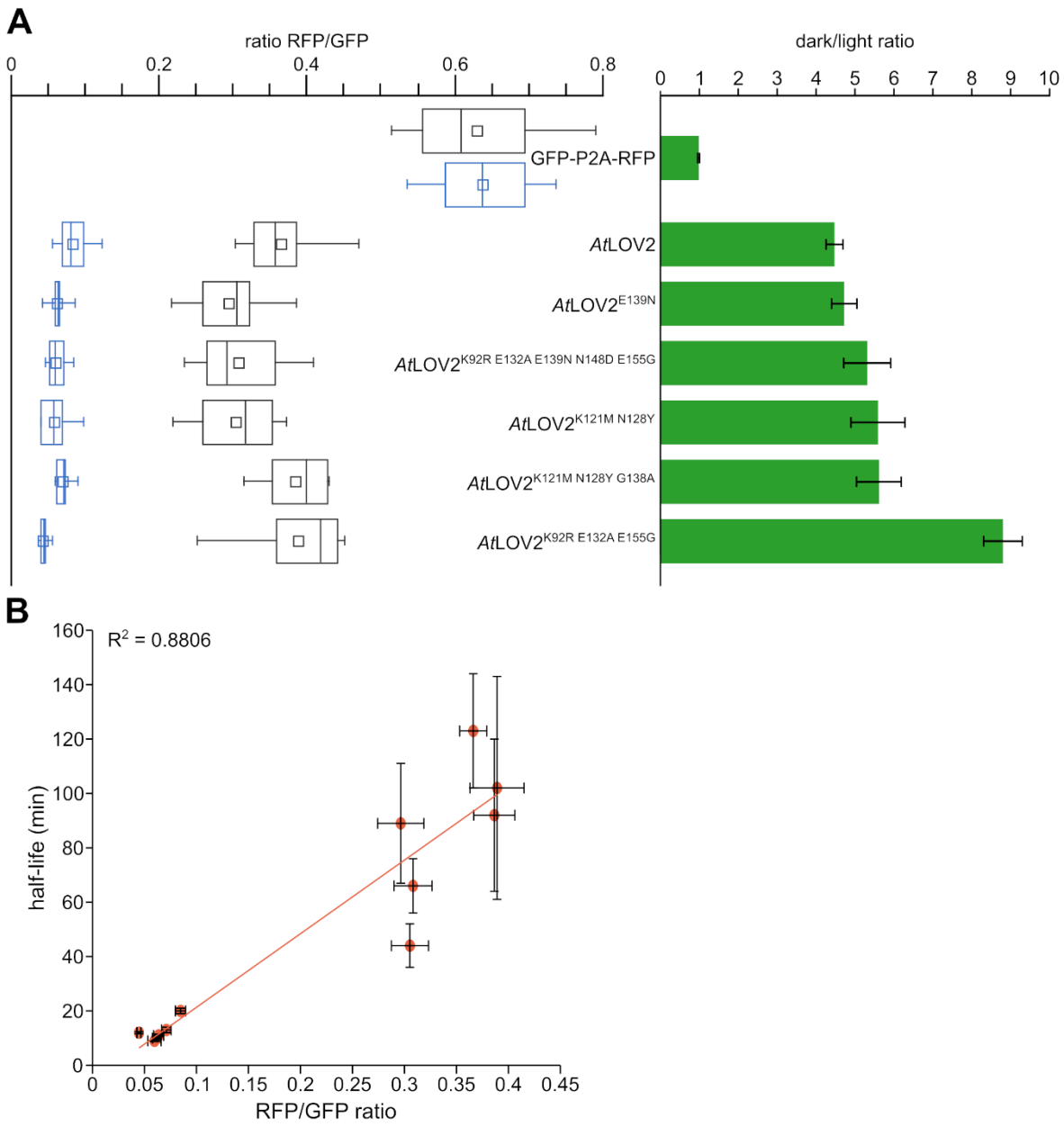

Supplemental Figure S3 Ratiometric measurement of psd abundance by fluorimeter measurements.

A) Fluorimeter measurements, same strains as in Supplemental Figure S2B. Left side: RFP/GFP ratio in darkness (black) or in cells exposed to blue-light (blue); right side: dark/light ratio. B) Correlation of half-life measurements of the psd variants measured by translational shut-off with cycloheximide[1] with the RFP/GFP ratios obtained by fluorimeter measurements shown in **A**. The high correlation indicates the usefulness of the ratiometric measurements to characterize abundance of psd variants.

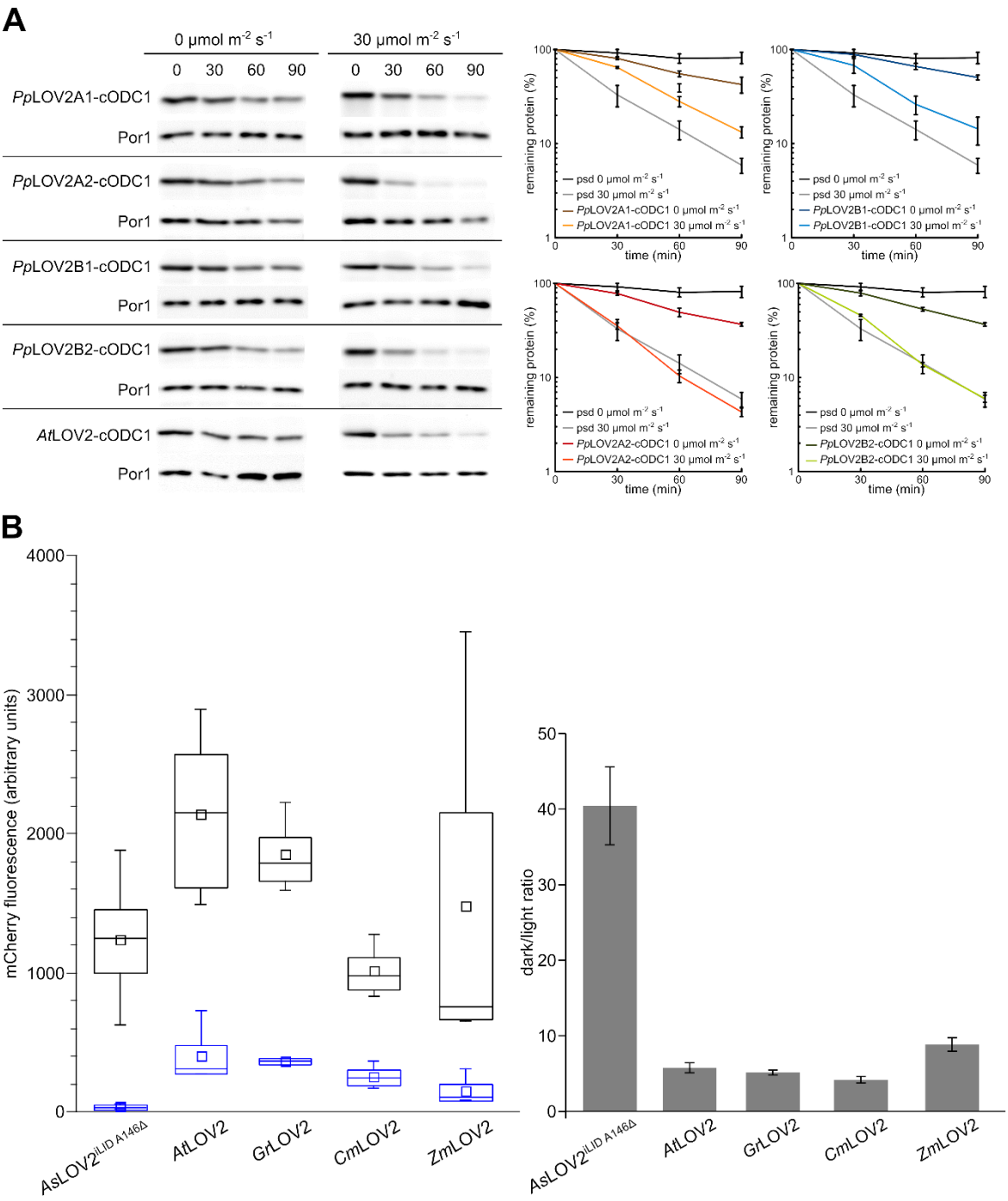

Supplemental Figure S4 Characterization of LOV2 domains in the context of the psd module.

A) Translational shut-off analysis of *At*LOV2-psd (pDS112) compared to *Pp*LOV2A1-psd (pDS150), *Pp*LOV2A2-psd (pDS149), *Pp*LOV2B1-psd (pDS147), and *Pp*LOV2B2-psd (pDS148). Cycloheximide was used to stop translation, stability of sfGFP-psd variants was characterized by immunoblotting. Cells were kept in darkness or exposed to blue-light (465 nm; 30 µmol m^{-2} s^{-1}) during the experiment. *Physcomitrella patens* LOV2 domains showed similar behavior as *At*LOV2. B) RFP fluorescence measurements of psd variants obtained by flow cytometry. RFP fluorescence in cells growing in darkness or exposed to blue-light are shown (left side). Dark/light ratio is shown in the right graph. None of the LOV2 domains shows a behavior as pronounced as the *As*LOV2$^{iLID\ A146\Delta}$ variant. Abbreviations: *As Avena sativa* (pDS219-2); *At Arabidopsis thaliana* (pDS185); *Gr Gossipium raimondii* (pLK9); *Cm Cucumis melo* (pLK10); *Zm Zea mays* (pLK15).

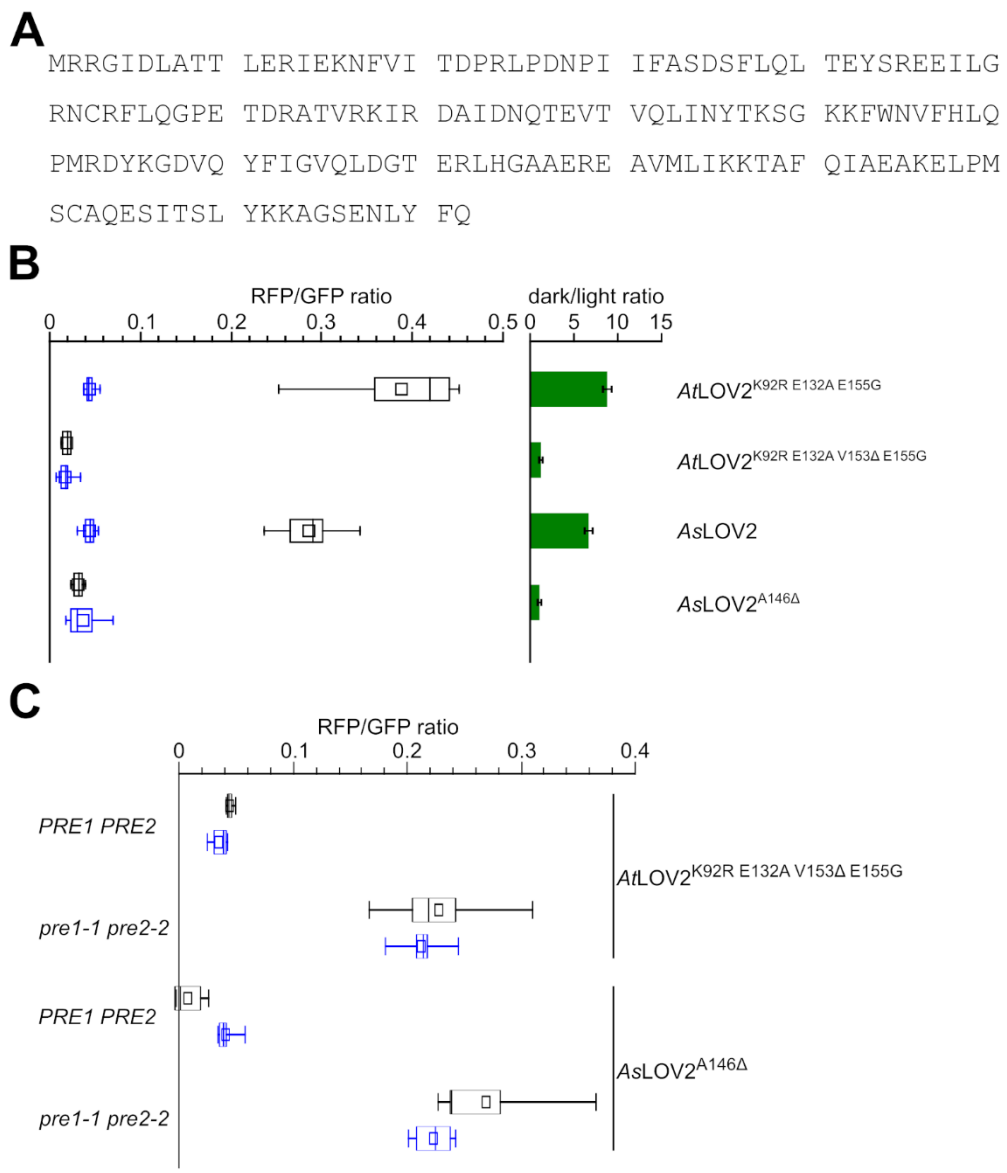

Supplemental Figure S5 Amino acid sequence of iLID$^{A146\Delta}$ and characterization of psd variants with a similar amino acid deletion.

A) Amino acid sequence of the *As*LOV2$^{iLID\ A146\Delta}$-psd construct. B) Left graph: RFP/GFP ratiometric measurement of psd module variants *At*LOV2$^{K92R\ E132A\ E155G}$ (pSH5), *At*LOV2$^{K92R\ E132A\ V153\Delta\ E155G}$ (pDS236), *As*LOV2 (pSH3), and *As*LOV2$^{A146\Delta}$ (pDS235) in darkness (black) or in cells exposed to blue-light (blue). Right graph: dark/light ratio. Yeast strain ESM356-1. C) RFP/GFP ratiometric measurements of *At*LOV2$^{K92R\ E132A\ V153\Delta\ E155G}$ and *As*LOV2$^{A146\Delta}$ in proteasome mutants (*pre1-1 pre2-2*; WCG4a-11/22) with reduced proteolytic capacity compared to control cells (*PRE1 PRE2*; WCG4a). The same plasmids were used as in **B**. Deletion of A153 in *At*LOV2$^{K92R\ E132A\ E155G}$ or A146 in *As*LOV2 in the context of the psd module results in non-functional modules that are constantly degraded by the proteasome.

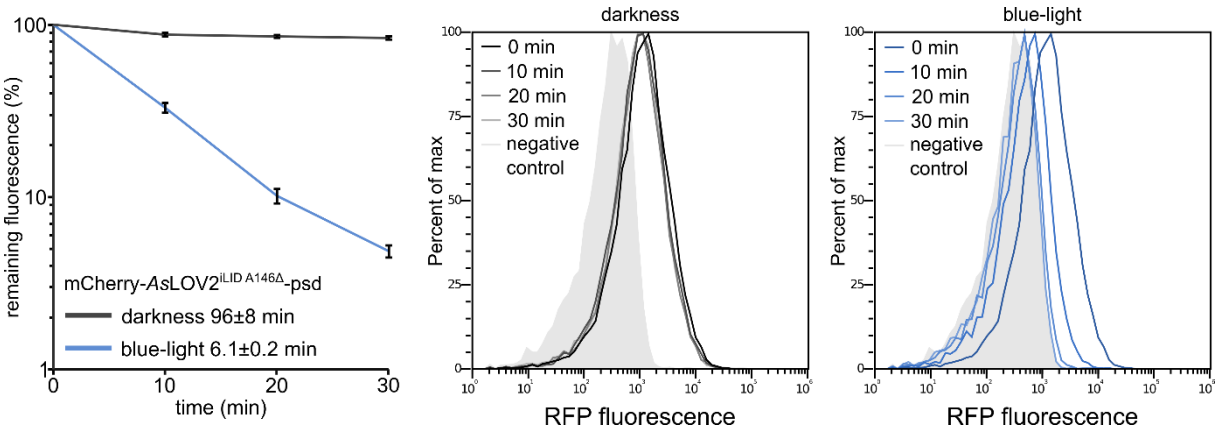

Supplemental Figure S6 Translational shut-off experiment of mCherry-iLID$^{A146\Delta}$-psd analyzed by flow cytometry.

The half-life of mCherry-iLID$^{A146\Delta}$-psd measured by flow cytometry is in darkness 96±8 min and in cells exposed to blue-light 6.1±0.2 min. The translational inhibitor cycloheximide was added to logarithmically growing yeast cells of strain ESM356-1 carrying pSH25 after removal of the first sample (t=0min). Cells were kept in darkness or exposed to blue-light (465 nm; 30 µmol m^{-2} s^{-1}). Samples were removed at the indicated time points and sodium azide (final concentration 10 mM) was added to each sample. RFP fluorescence was measured with a flow cytometer. Left graph: Quantification of several flow cytometry measurements (n=9) of mCherry-iLID$^{A146\Delta}$-psd (error bars: SEM). Middle graph: Example plot for cells kept in darkness during the experiment. Right graph: Example plot for the cells exposed to blue-light.

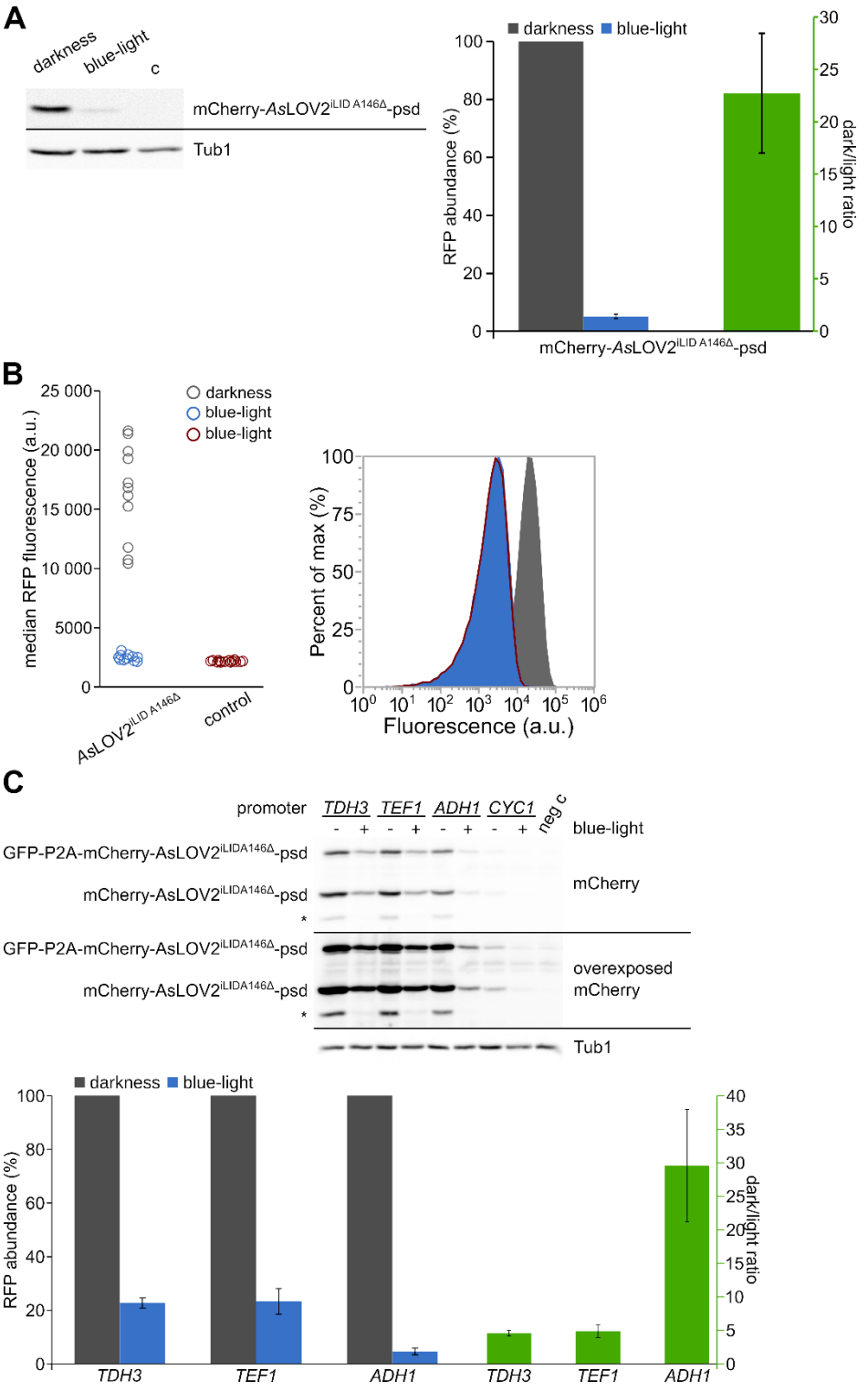

Supplemental Figure S7 Characterization of mCherry-*As*LOV2$^{iLID\ A146\Delta}$-psd in yeast.

A) Immunoblotting analysis of chromosomally integrated mCherry-*As*LOV2$^{iLID\ A146\Delta}$-psd (YSH6). Cells were grown in darkness or exposed to blue light (465 nm; 30 µmol m^{-2} s^{-1}). Cells were lysed by alkaline lysis method; antibodies used were directed against mCherry and Tub1 (loading control). Graph: quantification of RFP abundance and dark/light ratio (error bars: SEM). B) Flow cytometer measurements of chromosomally integrated mCherry-*As*LOV2$^{iLID\ A146\Delta}$-psd. Strain and growth conditions as in **A**. C) Immunoblotting analysis of plasmid encoded *GFP-P2A-mCherry-AsLOV2$^{iLID\ A146\Delta}$-psd* expressed by promoters of different strength. Yeast cells ESM356-1 containing plasmids pSH38 (*TDH3* promoter), pSH37

(*TEF1*), pDS219-2 (*ADH1*), and pSH36 (*CYC1*) were used for the analysis. Experimental conditions as in **A**. As the signals for the *CYC1* construct were close to the detection limit, we added a second exposure that is overexposed regarding the signals of the *TDH3*, *TEF1*, and *ADH1* constructs. This shows that the protein abundance for the *CYC1* construct in darkness is lower than the protein levels in the other constructs in cells exposed to blue-light. Please note that we observed two major signals by immunoblotting. The molecular weight corresponded to unseparated GFP-P2A-mCherry-*As*LOV2$^{iLID\ A146\Delta}$-psd and mCherry-*As*LOV2$^{iLID\ A146\Delta}$-psd (as indicated on the left). In some lanes another fragment appears (marked by *) that most likely corresponds to fragmented mCherry.[2] Graph: RFP abundance and dark/light ratio of the constructs shown in the immunoblot (n≥4; error bars: SEM).

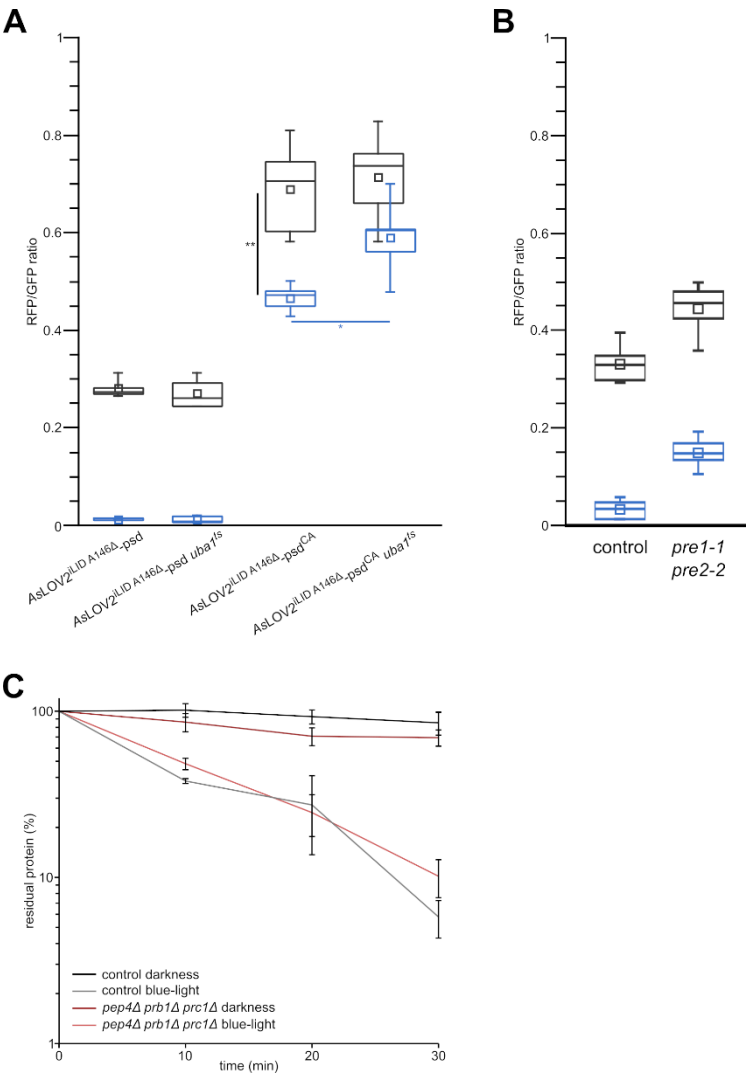

Supplemental Figure S8 Degradation of *As*LOV2$^{iLID\ A146\Delta}$-psd requires a functional cODC1 degron.

A) RFP/GFP ratiometric measurement of *As*LOV2$^{iLID\ A146\Delta}$-psd (pDS219-2) and *As*LOV2$^{iLID\ A146\Delta}$-psd^{CA} (pSH22) in a temperature sensitive *UBA1* allele (JD77; control JD47). The similar degradation behavior of mCherry-*As*LOV2$^{iLID\ A146\Delta}$-psd construct in cells with impaired ubiquitin activation indicates that ubiquitin-dependent proteolysis does not play a deciding role during its degradation. The cysteine to alanine exchange in the cODC1 degron part abolishes ubiquitin-independent degradation of the construct by the proteasome, which results in strong degradation impairment. The difference between *As*LOV2$^{iLID\ A146\Delta}$-psd^{CA} and *As*LOV2$^{iLID\ A146\Delta}$-psd^{CA} *uba1^{ts}* indicates that ubiquitin-dependent degradation might contribute to a certain degree in the proteolysis. Cells were shifted to 37°C 2 hours before the samples were collected. Other experimental conditions as described for Figure 1A. B) RFP/GFP ratiometric measurement of *As*LOV2$^{iLID\ A146\Delta}$-psd (pDS219-2) in a yeast strain with impaired proteasomal degradation (*pre1-1 pre2-2*; WCG11/22) compared to a wild type control (WCG4a). As expected, the *As*LOV2$^{iLID\ A146\Delta}$-psd construct showed lower degradation in the strain with impaired proteasomal degradation. Experimental conditions as described for Figure 1A. C) Determination of the half-life of RFP-*As*LOV2$^{iLID\ A146\Delta}$-psd in control cells (W303-1C) and cells with impaired vacuolar proteolysis (*pep4Δ prb1 Δ prc1 Δ*; CBO18) using the translation inhibitor cycloheximide. Experimental conditions as in Figure 1D. Blue-light induced degradation of RFP-*As*LOV2$^{iLID\ A146\Delta}$-psd was not considerably changed compared to the control (error bars: SEM).

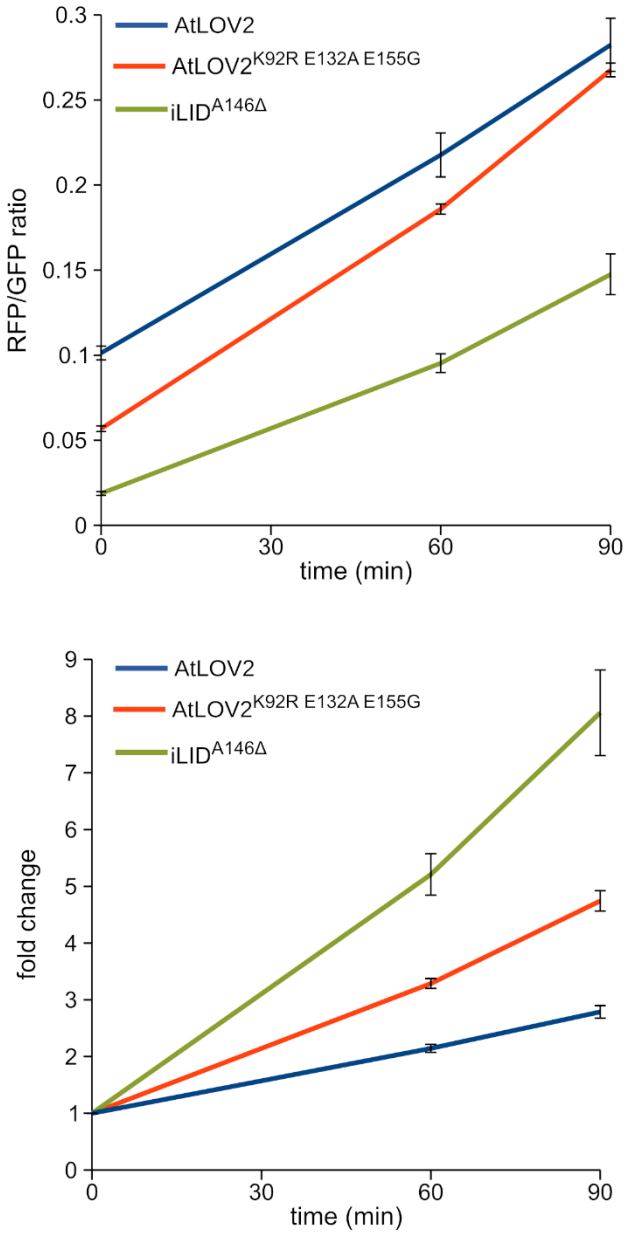

Supplemental Figure S9 Kinetics of psd abundance increase after transfer of cells from blue-light to darkness.

Ratiometric RFP/GFP fluorimeter measurements of *At*LOV2-psd (pDS185), *At*LOV2$^{K92R\ E132A\ E155G}$-psd (pSH5), and *As*LOV2$^{iLID\ A146\Delta}$-psd (pDS219-2). Upper graph: RFP/GFP ratios, lower graph: fold change over time (normalized RFP/GFP ratios to initial value).

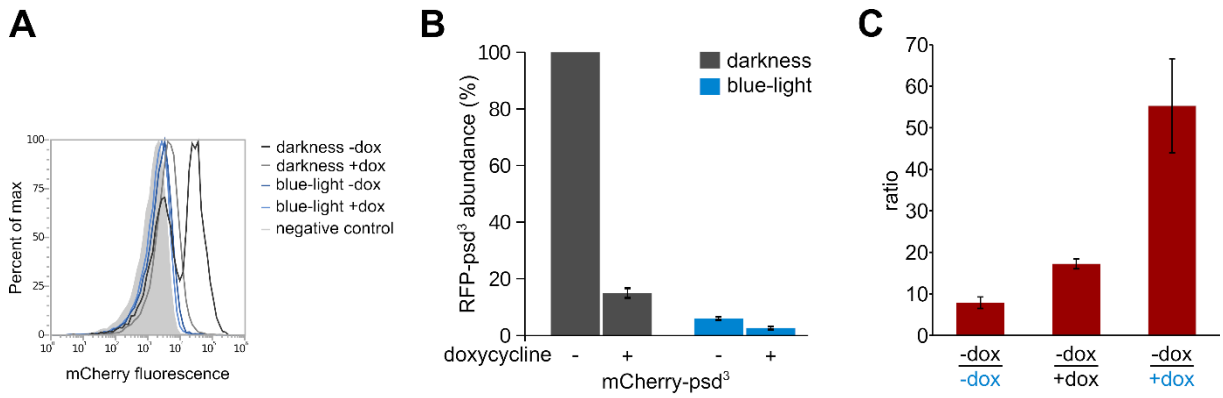

Supplemental Figure S10 Flow cytometry measurements of RFP-psd^3 controlled by the doxycycline promoter

The RFP fluorescence of ESM356-1 containing plasmid pDS239 was measured in cells exposed to the tetracycline-derivative doxycycline and blue-light or not. ESM356-1 containing pRS314 was used as negative control. Experimental conditions as described for Supplemental Figure S7B. A) Overlay of single RFP measurements of the strains at different conditions. B) Quantification of the RFP fluorescence normalized to cells kept in darkness in the absence of doxycycline. (n=13; error bar: standard error of the mean). C) Ratios of the different conditions (as indicated) of the measurements shown in B.

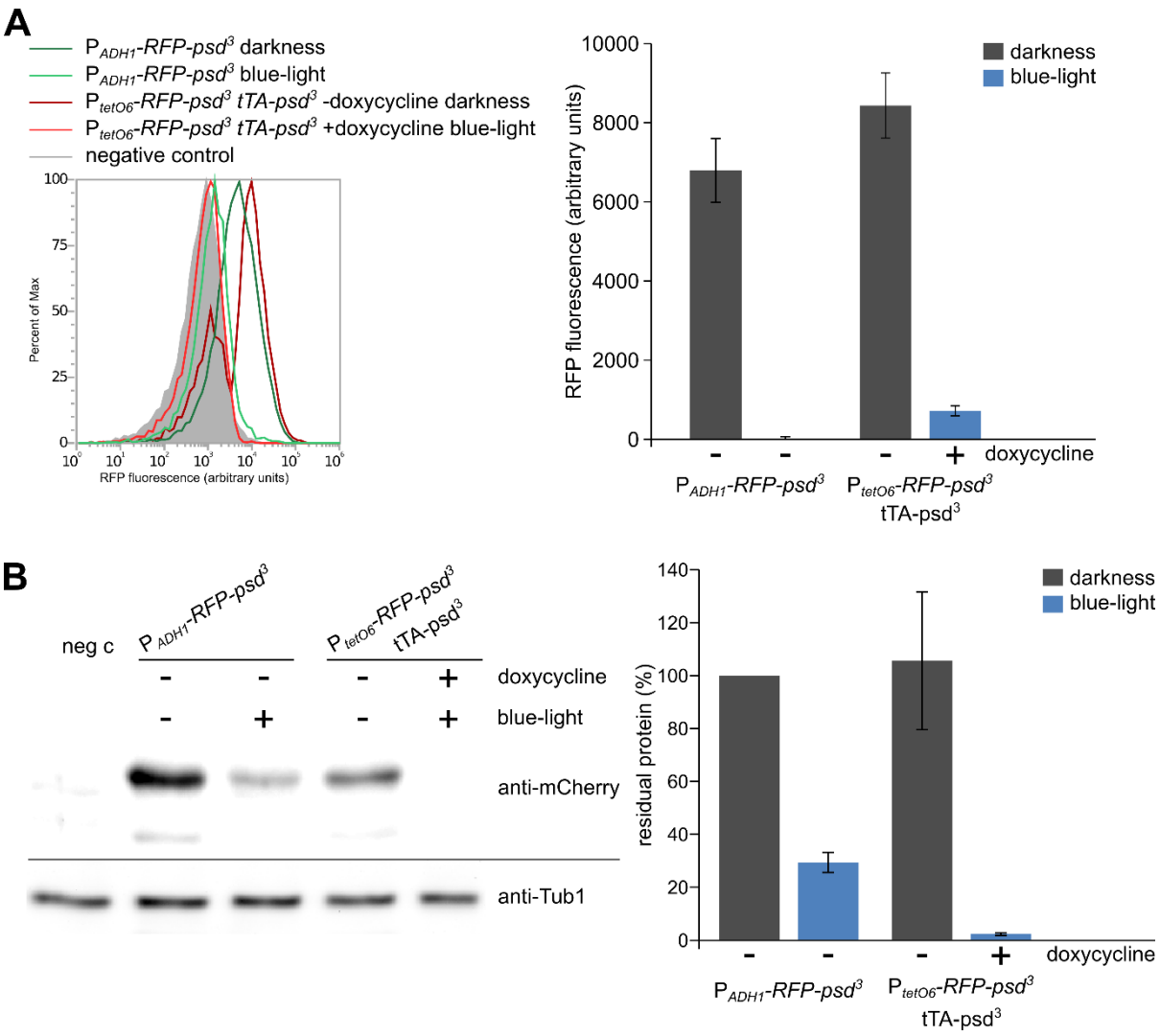

Supplemental Figure S11 Comparison of the synthetic doxycycline-regulatable promoter with the *ADH1* promoter

The RFP fluorescence of yeast cells (P_{ADH1}: ESM356-1 + pSH25; P_{tetO6}: ESM356-1 + pDS239) was quantified in the presence and absence of doxycycline and blue-light to compare the promoter strength in the absence of inducer. A) Flow cytometry measurements show comparable RFP fluorescence in both yeast strains in darkness and absence of doxycycline. Experimental conditions as described for Supplemental Figure S7B (n=6; error bar: SEM). B) Immunoblotting experiments show similar RFP signals in both yeast strains in darkness and absence of doxycycline. Experimental conditions as described for Supplemental Figure S7A (n=4; error bar: SEM).

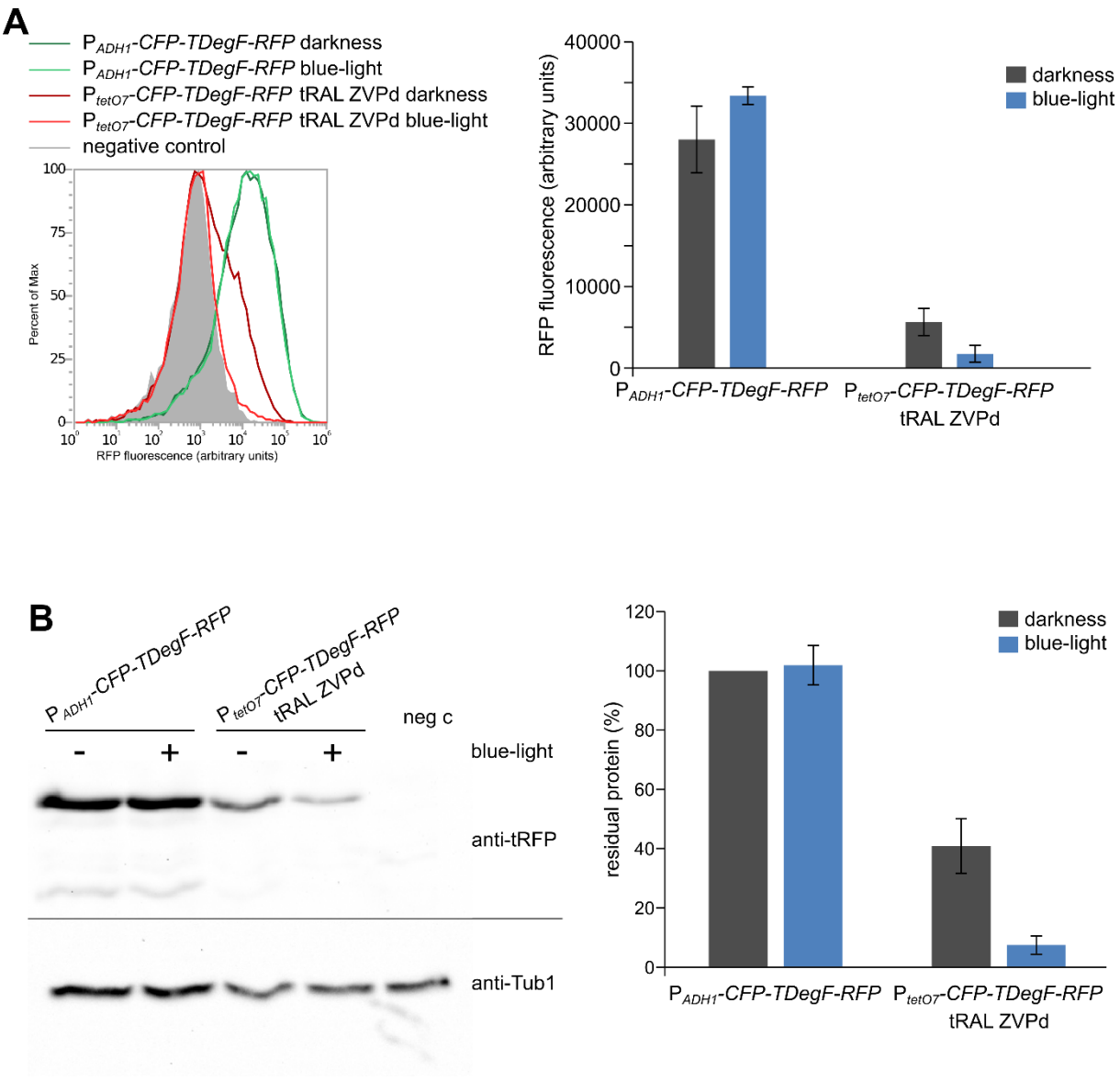

Supplemental Figure S12 CFP-TDegF-RFP abundance controlled by the psTF-regulated promoter compared with the *ADH1* promoter

The RFP fluorescence of yeast cells (P_{ADH1}: ESM356-1 + pDS7; P_{tetO6}: ESM356-1 + pSH32) was quantified in the presence and absence of blue-light to compare the promoter strength in the absence of inducer. A) Flow cytometry measurements revealed a reduction of RFP fluorescence in the psTF samples in darkness to 20 % compared to the *ADH1* promoter samples. Experimental conditions as described for Supplemental Figure S7B (n=6; error bar: SEM). B) Immunoblotting experiments show a reduction of RFP signals in darkness in the psTF samples to 40 % compared to the *ADH1* promoter. Experimental conditions as described for Supplemental Figure S7A (n=4; error bar: SEM).

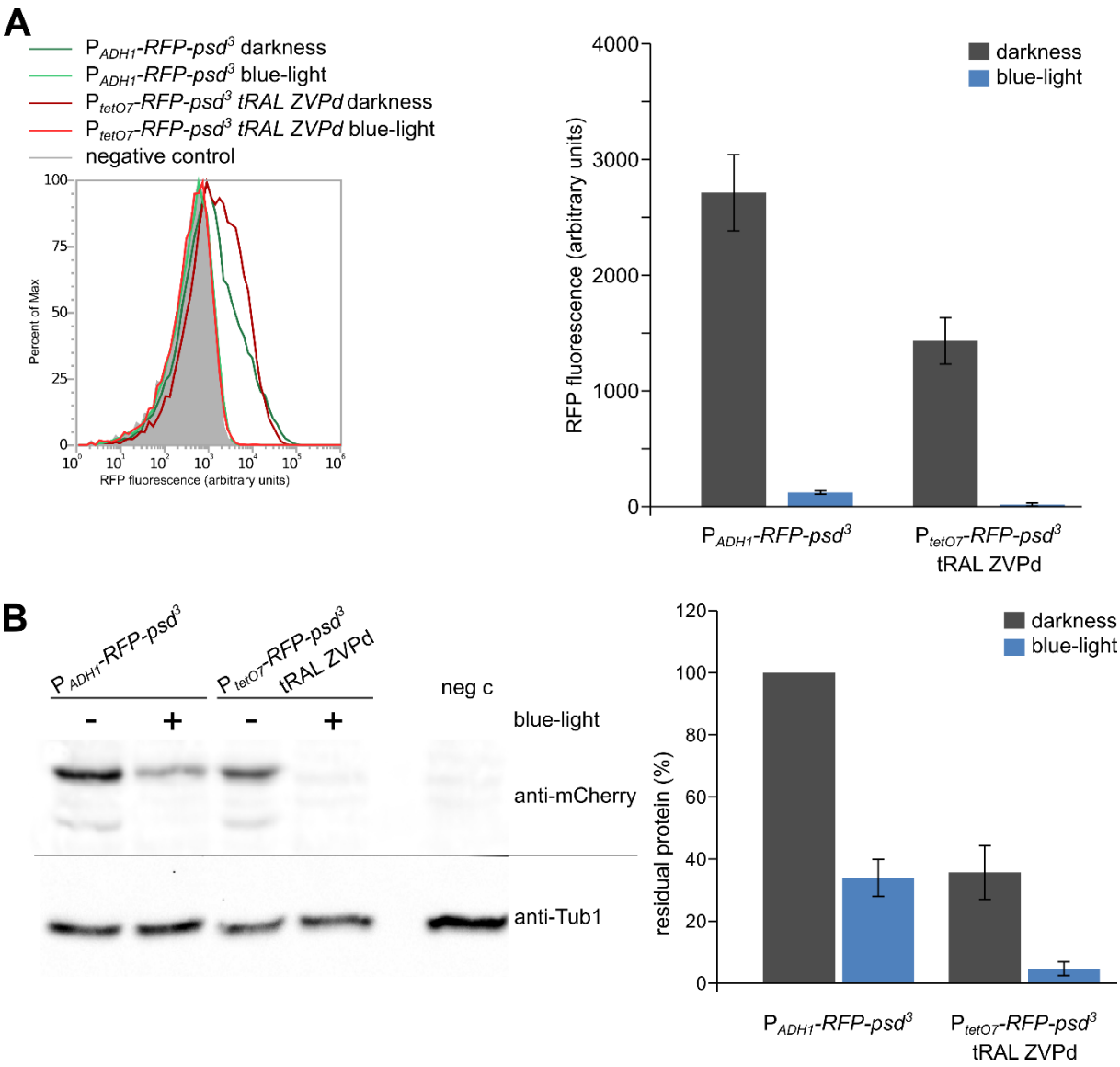

Supplemental Figure S13 RFP-psd^3 abundance controlled by the psTF-regulated promoter compared with the *ADH1* promoter

The RFP fluorescence of yeast cells (P_{ADH1}: ESM356-1 + pSH25; P_{tetO7}: ESM356-1 + pSH33) was quantified in the presence and absence of blue-light to compare the promoter strength in the absence of inducer. A) Flow cytometry measurements revealed a reduction of RFP fluorescence in the psTF samples in darkness to 50 % compared to the *ADH1* promoter samples. Experimental conditions as described for Supplemental Figure S7B (n=6; error bar: SEM). B) Immunoblotting experiments show a reduction of RFP signals in darkness in the psTF samples to 36 % compared to the *ADH1* promoter. Experimental conditions as described for Supplemental Figure S7A (n=4; error bar: SEM).

Supplemental Table S1: List of yeast strains

Name	genotype	source
ESM356-1	*MATa ura3-53 leu2-Δ1 his3-Δ200 trp1-Δ63*	[3]
YDS28	ESM356-1 pRS304-P_{HIS3}-*mCherry-TUB1*	[4]
YSH2	ESM356-1 *cdc48-mCherry-psd*^{3}*::kanMX*	this study
YSH1	YDS28 *cdc48-mCherry-psd*^{3}*::kanMX*	this study
YSH10	YDS28 *npl4-3myc-psd*^{3}*::kanMX*	this study
WCG4a	*MATa ura3 leu2-3,112 his3-11,15 Can*^{S} *Gal*$^{+}$	[5]
WCG11/22	WCG4a *pre1-1 pre2-2*	[5]
YSH6	*dit1Δ::natNT2::*P_{ADH1}-*GFP*-T_{DIT1} *leu2Δ::hphNT1::*P_{ADH1}-*mCherry-iLID*$^{A146\Delta}$*-cODC1*	this study
JD47-13C	*MATa his3-Δ200 leu2-3,112 lys2-801 trp1-Δ63 ura3-52*	[6]
JD77	JD47-13C *uba1Δ::HIS3* pRSts64-1 (*uba1*^{ts} *TRP1*)	[6]
W303-1A	*MATa ura3-1 his3-11,15 leu2-3,112 ade2-1 trp1-1 can1-100*	[7]
CBO18	W303-1A *pep4Δ::HIS3 prb1Δ::hisG prc1Δ::hisG*	[8]

Supplemental Table S2: List of plasmids

Name	genotype	source
pRS315	*LEU2 ARS209/CEN2 ori bla*	[9]
pRS314	*TRP1 ARS209/CEN2 ori bla*	[9]
pDS185	pRS315 P_{ADH1}-*sfGFP-P2A-mCherry-3myc-AtLOV2-cODC1*	this study
pSH5	pRS315 P_{ADH1}-*sfGFP-P2A-mCherry-3myc-AtLOV2*$^{K92R\ E132A\ E155G}$-*cODC1*	this study
pSH3	pRS315 P_{ADH1}-*sfGFP-P2A-mCherry-3myc-AsLOV2-cODC1*	this study
pDS219-1	pRS315 P_{ADH1}-*sfGFP-P2A-mCherry-iLID-cODC1*	this study
pDS219-2	pRS315 P_{ADH1}-*sfGFP-P2A-mCherry-iLID*$^{A146\Delta}$-*cODC1*	this study
pSH25	pRS315 P_{ADH1}-*mCherry-iLID*$^{A146\Delta}$-*cODC1*	this study
pDS228	pRS315 P_{ADH1}-$^{\Delta N}$*sic1-3myc-iLID*$^{A146\Delta}$-*cODC1*	this study
pDS229	pRS315 P_{CLB2}-*clb2*$^{\Delta DB}$-*3myc-iLID*$^{A146\Delta}$-*cODC1*	this study
pDS239	pRS314 P_{CYC1}-*tTA-iLID*$^{A146\Delta}$-*cODC1* $P_{tetO6GAL1core}$-*mCherry-iLID*$^{A146\Delta}$-*cODC1*	this study
pSH32	pRS314 P_{CYC1}-*HA-tetR-AsLOV2* P_{HIS3}-*Zdk1-VP16-3myc-iLID*$^{A146\Delta}$-*cODC1* $P_{tetO7GAL1core}$-*CFP-TDegF-mKate*	this study
pSH33	pRS314 P_{CYC1}-*HA-tetR-AsLOV2* P_{HIS3}-*Zdk1-VP16-3myc-iLID*$^{A146\Delta}$-*cODC1* $P_{tetO7GAL1core}$-*mCherry-iLID*$^{A146\Delta}$-*cODC1*	this study
pFMI14	pRS315 P_{ADH1}-*GFP-P2A-mCherry*	this study
pDS194	pRS315 P_{ADH1}-*GFP-mCherry-3myc-AtLOV2-cODC1*	this study
pSH11	pRS315 P_{ADH1}-*sfGFP-P2A-mCherry-3myc-AtLOV2*$^{K121M\ N128Y\ G138A}$-*cODC1*	this study
pSH5	pRS315 P_{ADH1}-*sfGFP-P2A-mCherry-3myc-AtLOV2*$^{K92R\ E132A\ E155G}$-*cODC1*	this study
pSH7	pRS315 P_{ADH1}-*sfGFP-P2A-mCherry-3myc-AtLOV2*$^{K121M\ N128Y}$-*cODC1*	this study
pSH1	pRS315 P_{ADH1}-*sfGFP-P2A-mCherry-3myc-AtLOV2*$^{K92R\ E132A\ E139N\ N148D\ E155G}$-*cODC1*	this study
pSH8	pRS315 P_{ADH1}-*sfGFP-P2A-mCherry-3myc-AtLOV2*^{E139N}-*cODC1*	this study
pDS112	pRS315 P_{ADH1}-*sfGFP-3myc-AtLOV2-cODC1*	this study
pDS150	pRS315 P_{ADH1}-*sfGFP-3myc-PpLOV2A1-cODC1*	this study
pDS149	pRS315 P_{ADH1}-*sfGFP-3myc-PpLOV2A2-cODC1*	this study
pDS147	pRS315 P_{ADH1}-*sfGFP-3myc-PpLOV2B1-cODC1*	this study
pDS148	pRS315 P_{ADH1}-*sfGFP-3myc-PpLOV2B2-cODC1*	this study
pLK9	pRS315 P_{ADH1}-*mCherry-GrLOV2-cODC1*	this study
pLK10	pRS315 P_{ADH1}-*mCherry-CmLOV2-cODC1*	this study
pLK15	pRS315 P_{ADH1}-*mCherry-ZmLOV2-cODC1*	this study
pDS236	pRS315 P_{ADH1}-*sfGFP-P2A-mCherry-3myc-AtLOV2*$^{K92R\ E132A\ V153\Delta\ E155G}$-*cODC1*	this study
pDS235	pRS315 P_{ADH1}-*sfGFP-P2A-mCherry-3myc-AsLOV2*$^{A146\Delta}$-*cODC1*	this study
pSH22	pRS315 P_{ADH1}-*sfGFP-P2A-mCherry-iLID*$^{A146\Delta}$-*cODC1*^{CA}	this study
pDS168	pRS315 P_{ADH1}-*mCherry-AtLOV2-cODC1*	this study
pDS7	pRS314 P_{ADH1}-*CFP-TDegF-mKate*	[10]
pSH36	pRS315 P_{CYC1}-*sfGFP-P2A-mCherry-iLID*$^{A146\Delta}$-*cODC1*	this study
pSH37	pRS315 P_{TEF1}-*sfGFP-P2A-mCherry-iLID*$^{A146\Delta}$-*cODC1*	this study
pSH38	pRS315 P_{TDH3}-*sfGFP-P2A-mCherry-iLID*$^{A146\Delta}$-*cODC1*	this study

References

1. Usherenko, S., Stibbe, H., Muscò, M., Essen, L. O., Kostina, E. A., and Taxis, C. (2014) Photo-sensitive degron variants for tuning protein stability by light. *BMC Syst. Biol. 8*, 128.

2. Baird, G. S., Zacharias, D. a, and Tsien, R. Y. (2000) Biochemistry, mutagenesis, and oligomerization of DsRed, a red fluorescent protein from coral. *Proc. Natl. Acad. Sci. U. S. A. 97*, 11984–9.

3. Pereira, G., Tanaka, T. U., Nasmyth, K., and Schiebel, E. (2001) Modes of spindle pole body inheritance and segregation of the Bfa1p-Bub2p checkpoint protein complex. *EMBO J. 20*, 6359–6370.

4. Jungbluth, M., Renicke, C., and Taxis, C. (2010) Targeted protein depletion in Saccharomyces cerevisiae by activation of a bidirectional degron. *BMC Syst. Biol. 4*, 176.

5. Heinemeyer, W., Gruhler, A, Möhrle, V., Mahé, Y., and Wolf, D. H. (1993) PRE2, highly homologous to the human major histocompatibility complex-linked RING10 gene, codes for a yeast proteasome subunit necessary for chrymotryptic activity and degradation of ubiquitinated proteins. *J. Biol. Chem. 268*, 5115–20.

6. Palanimurugan, R., Scheel, H., Hofmann, K., and Dohmen, R. J. (2004) Polyamines regulate their synthesis by inducing expression and blocking degradation of ODC antizyme. *EMBO J. 23*, 4857–4867.

7. Thomas, B. J., and Rothstein, R. (1989) Elevated recombination rates in transcriptionally active DNA. *Cell 56*, 619–630.

8. Graham, T. R., and Emr, S. D. (1991) Compartmental organization of Golgi-specific protein modification and vacuolar protein sorting events defined in a yeast sec18 (NSF) mutant. *J. Cell Biol. 114*, 207–18.

9. Sikorski, R. S., and Hieter, P. (1989) A system of shuttle vectors and yeast host strains designed for efficient manipulation of DNA in Saccharomyces cerevisiae. *Genetics 122*, 19–27.

10. Taxis, C., Stier, G., Spadaccini, R., and Knop, M. (2009) Efficient protein depletion by genetically controlled deprotection of a dormant N-degron. *Mol. Syst. Biol. 5*, 267.